

Imprints of an extended Chevallier-Polarski-Linder parametrization on the large scale of our universe

Supriya Pan,^{1,*} Weiqiang Yang,^{2,†} and Andronikos Paliathanasis^{3,‡}

¹*Department of Mathematics, Presidency University, 86/1 College Street, Kolkata 700073, India*

²*Department of Physics, Liaoning Normal University, Dalian, 116029, P. R. China*

³*Institute of Systems Science, Durban University of Technology,
PO Box 1334, Durban 4000, Republic of South Africa*

In the present work we perform a systematic analysis of a new dark energy parametrization and its various corrections at first and higher orders around the present epoch $z = 0$, where the first order correction of this dark energy parametrization recovers the known Chevallier-Polarski-Linder model. We have considered up to the third order corrections of this parametrization and investigate the models at the level of background and perturbations. The models have been constrained using the latest astronomical datasets from a series of potential astronomical data, such as the cosmic microwave background observations, baryon acoustic oscillations measurements, recent Pantheon sample of the supernova type Ia and the Hubble parameter measurements. From the analyses we found that all parametrization favor the quintessential character of the dark energy equation of state where the phantom crossing is marginally allowed (within 68% CL). Finally, we perform the Bayesian analysis using `MCEvidence` to quantify the statistical deviations of the parametrizations compared to the standard Λ CDM cosmology. The Bayesian analysis reports that Λ CDM is favored over all the DE parametrizations.

PACS numbers: 98.80.-k, 95.35.+d, 95.36.+x

1. INTRODUCTION

According to the theory of general relativity, one possible way to describe the recent observational evidences is to introduce the dark energy, a hypothetical fluid with large negative pressure [1]. However, apart from this negativity condition on the pressure of dark energy, no one knows what exactly this particular fluid is. The simplest explanation to the dark energy theory comes through the introduction of positive cosmological constant, Λ , which does not evolve with the time. But, the cosmological constant already suffers from two major problems, one which is recognized as the cosmological constant problem and the other is the cosmic coincidence problem. Thus, although as stated by a series of observational data, the Λ -cosmology is an elegant version to model the recent observational features of the universe, the problems associated with the above motivate us to think of the scenarios beyond the standard Λ -cosmology paradigm.

The simplest extension to Λ -cosmology is the w_x -cosmology in which w_x is the dark energy equation-of-state quantified as the ratio of pressure to its density, mathematically which is $w_x = p_x/\rho_x$. One can identify that p_x and ρ_x are respectively the pressure and energy density of the dark energy fluid. The equation-of-state w_x being -1 recovers the Λ -cosmology. In general one can assume $w_x (\neq -1)$ to be either time independent or dependent while the latter scenario is the most general

one. Thus, in the present work we shall focus on the alternative cosmologies to the Λ -cosmology in which the dark energy equation-of-state is evolving with the expansion of the universe.

The parametrization of w_x could be any function of the redshift z or the scale factor $a(t)$ of the Friedmann-Lemaître-Robertson-Walker universe; note that, $1 + z = a_0/a(t)$, where a_0 is the present value of the scale factor in this universe. Thus, since $w_x \equiv w_x(z) \equiv w_x(a)$ could be any arbitrary function of the redshift or the scale factor, therefore, in principle this gives us a complete freedom to pick up any particular model of interest and test it with the observational data in order to see whether that model is able to correctly describe the evolution of the universe. In fact one can realize that the introduction of the dark energy equation-of-state is a reverse mechanism to probe the expansion history of the universe. Going back to literature, one can find that this particular area of cosmology has been investigated well both at the level of background and perturbations where various parametrizations for w_x were introduced earlier [2–12] and later [13–42]. Precisely, the dark energy parametrization with only a single free parameter, with two free parameters, with three free parameters and finally with more than three parameters have been rigorously studied by various investigators.

The aim of the present work is slightly different. Here, we are considering an exponential dark energy parametrization that in its first order approximation around $z = 0$ recovers the CPL parametrization, and further we allow its higher order corrections in order to investigate how such extended corrections affect the evolution of the universe both at the level of background and perturbations. More specifically, we consider upto

*Electronic address: supriya.maths@presiuniv.ac.in

†Electronic address: d11102004@163.com

‡Electronic address: anpaliat@phys.uoa.gr

the third order expansion of the exponential dark energy model. We remark that in general every analytic function for the equation-of-state parameter around the $z = 0$ describes the CPL parametrization in the first correction; however, while we want to assume a general Taylor expansion of an analytic function $f(a)$ around $a = 1$, i.e. $f(a) = \sum_{i=0}^{\infty} w_i (a - 1)^i$, every new term which is introduced in the correction provides a new degree of freedom, a free parameter, in the model. Consequently, the models will have different degrees of freedom and they will not be in comparison. Hence, special relations amount the constants w_i should be considered, and for our analysis we assume that w_0 is free while $w_j = \frac{w_1}{j!}$, which $j \neq 0$, in which $f(a)$ is now the exponential function. However, by this approach we will get a remarkable information on how the nonlinear terms in the parametrizations of the equation-of-state affect the viability of the model in higher-redshifts.

The work has been organized in the following way. In section 2 we introduce the models for $w_x(z)$ and describe the general equations at the level of background and perturbations. After that in section 3 we provide an equivalence of the present dark energy parametrizations with the scalar field theory. Then in section 4 we describe the observational data and the statistical analysis that are used to constrain the models. After that in section 5 we describe the observational constraints extracted from the models using the astronomical data described in section 4. Then in section 6 we compute the evidences of the dark energy parametrizations through the `MCEvidence`. Finally, we close the work in section 7 with a brief summary of everything.

2. BASIC EQUATIONS AND THE MODELS

Considering a spatially flat Friedmann-Lemaître-Robertson-Walker line element $ds^2 = -dt^2 + a^2(t) \sum_{i=1}^3 dx_i^2$ (where $a(t)$ is the expansion scale factor of the universe), in the context of the Einstein gravity, we assume that (i) matter is minimally coupled to gravity, (ii) there is no interaction between any two fluids under consideration and (iii) all the fluids satisfy barotropic equation of state, i.e., $p_i = w_i \rho_i$ in which w_i being the barotropic state parameter for the i -th fluid having (ρ_i, p_i) as its the energy density and pressure, respectively. Precisely, we consider that the total energy density of the universe is, $\rho_{tot} = \rho_r + \rho_b + \rho_c + \rho_x$ and the total pressure thus becomes $p_{tot} = p_r + p_b + p_c + p_x$. Here, the subscripts r , b , c and x respectively stands for radiation, baryons, cold dark matter and dark energy. Thus, the barotropic indices are, $w_r = 1/3$, $w_b = w_c = 0$ and we assume w_x to be dynamical. The Einstein's field equations for the above FLRW universe can be written down as

$$H^2 = \frac{8\pi G}{3} \rho_{tot}, \quad (1)$$

$$\dot{H} = -4\pi G(p_{tot} + \rho_{tot}), \quad (2)$$

in which an overhead dot represents the cosmic time differentiation and $H \equiv \dot{a}/a$ is the Hubble rate of this universe. Now, using (1) and (2) (or alternatively the Bianchi's identity), one can find the balance equation

$$\dot{\rho}_{tot} + 3H(\rho_{tot} + p_{tot}) = 0. \quad (3)$$

Now, since as we assumed that we don't have any interaction between any two fluids of the universe, thus, they should satisfy their own conservation equation leading to

$$\dot{\rho}_i + 3H(\rho_i + p_i) = 0, \quad (4)$$

from which using the relation between pressure and energy density for the radiation, baryons, and cold (pressureless-) dark matter, one can find that $\rho_r = \rho_{r0} a^{-4}$, $\rho_m = \rho_b + \rho_c = (\rho_{b0} + \rho_{c0}) a^{-3}$. Here, ρ_{i0} is the present value of ρ_i . And finally, the evolution of the dark energy fluid can be given by,

$$\rho_x = \rho_{x0} \left(\frac{a}{a_0} \right)^{-3} \exp \left(-3 \int_{a_0}^a \frac{w_x(a')}{a'} da' \right), \quad (5)$$

where ρ_{x0} being the current value of ρ_x and a_0 is the present value of the scale factor that we set to be unity ($a_0 = 1$) without any loss of generality. We further note that the scale factor is related to the redshift that we shall frequently use hereafter via $1 + z = a_0/a = 1/a$. Thus, once the dark energy equation of state is prescribed, the evolution of the dark energy density can be found.

As we discussed above, we consider that the dark energy fluid follows a general parametrization in the following way:

$$w_x(z) = (w_0 - w_a) + w_a \exp \left(\frac{z}{1+z} \right) \quad (6)$$

where w_0 is the present value of the dark energy equation of state, that means, $w_x(z = 0) = w_0$ and w_a is another free parameter. The model (6) is very interesting by its construction since one can easily recognize that it could return a number of interesting parametrization that includes the classic Chevallier-Polarski-Linder parametrization $w_x(z) = w_0 + w_a z / (1+z)$ if we take the first approximation of the exponential function in (6).

We expand the exponential function of (6) upto its first, second and third order corrections leading to the following class of dark energy parametrization:

$$w_x(a) = w_0 + w_a \frac{z}{1+z}, \quad (7)$$

$$w_x(a) = w_0 + w_a \left[\frac{z}{1+z} + \frac{1}{2!} \left(\frac{z}{1+z} \right)^2 \right], \quad (8)$$

$$w_x(a) = w_0 + w_a \left[\frac{z}{1+z} + \frac{1}{2!} \left(\frac{z}{1+z} \right)^2 + \frac{1}{3!} \left(\frac{z}{1+z} \right)^3 \right], \quad (9)$$

and for convenience we call the dark energy parametrization of equations (7), (8) and (9) as “Extension 1” (Ext1 in short), “Extension 2” (Ext2 in short) and “Extension 3” (Ext3 in short), respectively. Let us note that in the above cases we have not considered the pivot redshift [39]. However, the consideration of pivoting redshift might be an interesting issue for investigations because as already commented in [39], one can find a specific value of the pivot redshift where the parameters w_0 and w_a are uncorrelated.

At the end of this section, we would like to present the qualitative features of the present dark energy parametrizations in terms of the evolution of their equations of state and the deceleration parameters. In order to do so, we assumed three different values of w_0 , namely, $w_0 = -0.95$, $w_0 = -1$ and $w_0 = -1.1$ and in each case we consider various values of w_a to understand how the curves behave with the increasing of the w_a parameter. In Fig. 1 we show the evolution of the dark energy parameterizations (6), (7), (8) and (9) setting the present value of the dark energy equation of state at $w_0 = 0.95$ where we allow different values of w_a such as $w_a = -0.3, -0.2, -0.1, 0, 0.1, 0.2, 0.3$. The curve with $w_a = 0$ simply returns $w = w_0$ and this has been kept to compare with other cruves having $w_a \neq 0$. From Fig. 1, we notice that for $w_a < 0$, the dark energy equation of state allows its phantom character which is much pronounced at high redshifts, while for $w_a > 0$, the reverse scenario is found. In a similar fashion, we investiagted the other cases with $w_0 = -1$ and $w_0 = -1.1$, however, we did not observe any significant changes in the qualitative evolution of $w_x(z)$, so we did not include the other figures.

We then plot the evolution of the deceleration parameter for all the DE parametrizations, namely, (6), (7), (8) and (9). Here we again assumed three fixed values of w_0 , namely, $w_0 = -0.95, -1, -1.1$ and in each case we assume different values of w_a similar to what we have shown in Fig. 1. Finally, we analyzed the evolution of the deceleration parameter for all the cases and found that all three cases return almost similar dynamics. That is why choose the case with for $w_0 = -0.95$ and exclude the others. The Fig. 2 corresponds to the case $w_0 = -0.95$. From this figure one can see that irrespective of the values of w_0 , a fine transition from the past decelerating phase to the current accelerating one is observed. The interest-

ing and important point in Fig. 2 is that, for negative values of w_a the transition redshifts are shifting towards higher redshifts (although mild) while for positive values of w_a , we see the reverse, that means the transition redshifts are shifting towards lower values of the redhft.

Overall, we find that the models at the level of background do not exhibit any deviations from one another. This is not surprising because the deviations between the cosmological models are usually reflected from their analysis at the level of perturbations. In what follows we shall consider the perturbation equations for all the DE parametrizations in this work.

We start with the following metric which is the perturbed form of the FLRW line element:

$$ds^2 = a^2(\eta) [-d\eta^2 + (\delta_{ij} + h_{ij})dx^i dx^j],$$

Here, η denotes the conformal time; δ_{ij} , h_{ij} are the unperturbed and the perturbative metric tensors, respectively. Now, considering the perturbed Einstein’s field equations, for a mode with wave-number k one can write down [43–45]:

$$\delta'_i = -(1 + w_i) \left(\theta_i + \frac{h'}{2} \right) - 3\mathcal{H} \left(\frac{\delta p_i}{\delta \rho_i} - w_i \right) \delta_i - 9\mathcal{H}^2 \left(\frac{\delta p_i}{\delta \rho_i} - c_{a,i}^2 \right) (1 + w_i) \frac{\theta_i}{k^2}, \quad (10)$$

$$\theta'_i = -\mathcal{H} \left(1 - 3 \frac{\delta p_i}{\delta \rho_i} \right) \theta_i + \frac{\delta p_i / \delta \rho_i}{1 + w_i} k^2 \delta_i - k^2 \sigma_i, \quad (11)$$

where $\delta_i = \delta \rho_i / \rho_i$ is the density perturbation for the i -th fluid; δ_i prime associated to any quantity denotes the derivatives with respect to conformal time; $\mathcal{H} = a'/a$ is the conformal Hubble parameter; $\theta_i \equiv ik^j v_j$ is the divergence of the i -th fluid velocity; $h = h_j^j$, is the trace of the metric perturbations h_{ij} ; σ_i denotes the anisotropic stress related to the i -th fluid. Let us also note that $c_{a,i}^2 = \dot{p}_i / \dot{\rho}_i$, is the adiabatic speed of sound of the i -th fluid which can also be written in terms of other physical quantities as $c_{a,i}^2 = w_i - \frac{w'_i}{3\mathcal{H}(1+w_i)}$, where we fix the sound speed $c_s^2 = \delta p_i / \delta \rho_i$ to be unity. Finally, we also note that we have neglected the anisotropic stress from the system for simplicity.

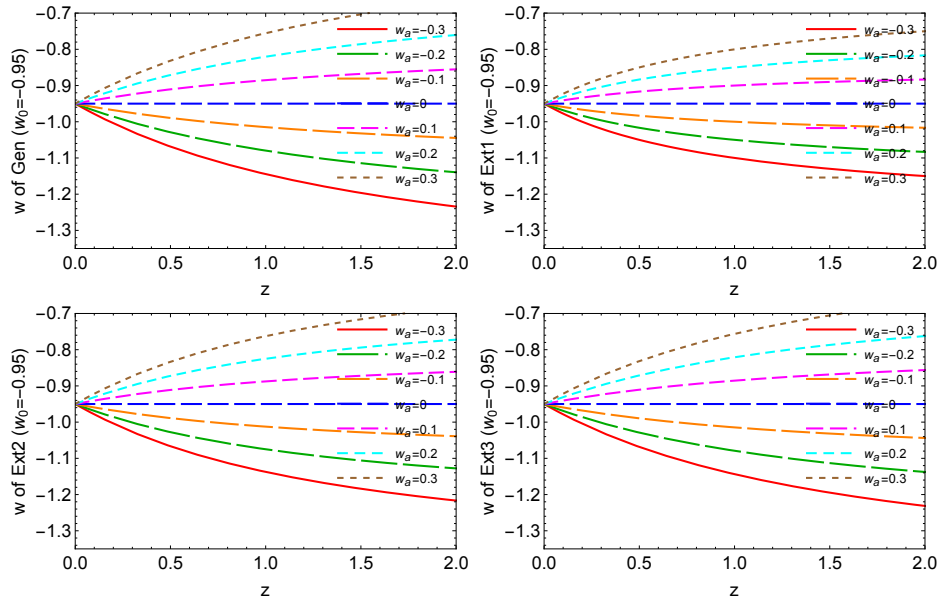


FIG. 1: We show the evolution of the dark energy parametrizations for different values of w_a with a fixed value of $w_0 = -0.95$

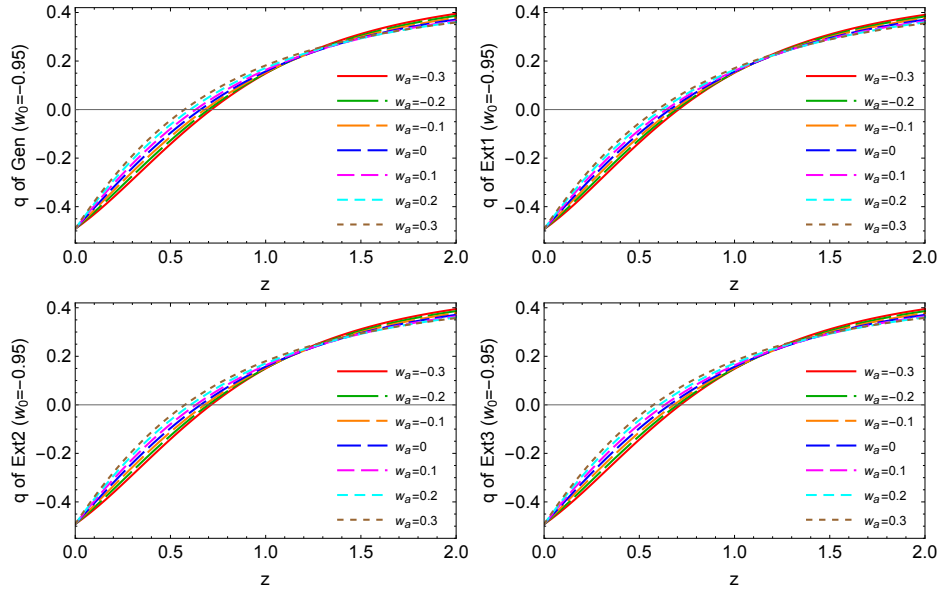


FIG. 2: The evolution of the deceleration parameter depicting a clear transition from the past decelerating phase to the current accelerating phase for all the dark energy models has been presented for different values of w_a and with a fixed value of $w_0 = -0.95$. One can easily notice that as long as w_a increase from its negative to positive values, the transition redshift shifts more closer to the present epoch.

3. SCALAR-FIELD DESCRIPTION

This section is devoted to provide with an equivalent field theoretic description for the dark energy parametrizations. A method to construct the scalar field potential which describe a given equation of state parameter was presented in [46]. Specifically, for a spatially flat FLRW as in the case of consideration, with a line element

$$ds^2 = -e^{F(\omega)} d\omega^2 + e^{\omega/3} \left[\frac{dr^2}{1 - Kr^2} + r^2 d\theta^2 + r^2 \sin^2 \theta d\phi^2 \right], \quad (12)$$

where $e^{F(\omega)}$ plays the role of a lapse function, the scale factor $a(\omega) = e^{\omega/3}$ and K is the curvature scalar of the universe. The exact solution of the scalar field and the

scalar field potential in case of vacuum are

$$\phi(\omega) = \pm \frac{\sqrt{6}}{6} \int \sqrt{F'(\omega)} d\omega, \quad (13)$$

$$V(\omega) = \frac{1}{12} e^{-F(\omega)} (1 - F'(\omega)) \quad (14)$$

or, equivalently, for the physical parameters, such as energy density and pressure

$$\rho_\phi(\omega) = \frac{1}{12} e^{-F(\omega)}, \quad P_\phi(\omega) = \frac{1}{12} e^{-F(\omega)} (2F'(\omega) - 1). \quad (15)$$

Consequently, for the latter definitions it follows

$$w_\phi(\omega) = \frac{P_\phi(\omega)}{\rho_\phi(\omega)} = (2F'(\omega) - 1). \quad (16)$$

Hence, for a specific equation of state parameter $w_\phi(\omega)$ the latter first-order equation can be solved and we can

determine the function $F(\omega)$. Subsequently, by replacing $F(\omega)$ in eqns. (13), (14) one can find the functional form of $V(\phi)$. For the general functional form of the equation of state, namely, eqn. (6), $w_x(\omega) = w_0 - w_a + w_a \exp(1 - e^{\omega/3})$, we find that

$$F(\omega) = \frac{1}{2}(1 + w_0 - w_a)\omega + \frac{1}{2}w_a \int \exp(1 - e^{\omega/3}) d\omega + F_0, \quad (17)$$

where F_0 is the constant of integration. Now, using the value of $F(\omega)$, one can find that

$$\phi(\omega) = \frac{1}{\sqrt{2}} \int \sqrt{1 + w_0 - w_a + w_a \exp(1 - e^{\omega/3})} d\omega, \quad (18)$$

and $V(\omega)$ can be solved as

$$V(\omega) = \frac{1}{24} \left(-e^{e^{\omega/3}} (w_0 + w_a - 1) - e w_a \right) \exp \left(-\frac{3e}{2} w_a \text{Ei}(-e^{\omega/3}) - \frac{\omega}{2} (w_0 + w_a + 1) - e^{\omega/3} \right), \quad (19)$$

where the symbol ‘Ei’ represents the exponential integral. For the CPL potential $w_x(\omega) = w_0 + w_a(1 - e^{\omega/3})$ we find

$$F(\omega) = \frac{1}{2}(1 + w_0 + w_a)\omega - \frac{3}{2}w_a e^{\omega/3} + F_0,$$

where F_0 is the integration constant and consequently we find that

$$\frac{\phi(\omega)}{\sqrt{3}} = \sqrt{w_a(e^{\omega/3} - 1) - (1 + w_0)} - \sqrt{1 + w_0 + w_a} \\ \times \arctan \sqrt{\frac{w_a(e^{\omega/3} - 1) - (1 + w_0)}{1 + w_0 + w_a}} \quad (20)$$

$$V(\omega) = \frac{1}{24} e^{F_0} \exp \left(\frac{3}{2} w_a e^{\omega/3} - \frac{1}{2} (1 + w_0 + w_a) \right) \\ \times \left(1 - w_0 + w_a (e^{\omega/3} - 1) \right). \quad (21)$$

For the Ext2 and Ext3 models the corresponding functions $F(\omega)$ are derived to be

$$F_{Ext}^2(\omega) = F_0 + \frac{1}{4} \left((2 + 2w_0 + 3w_a)\omega - 12w_a e^{\omega/3} + \frac{3}{2}w_a e^{2\omega/3} \right), \quad (22)$$

$$F_{Ext}^3(\omega) = F_0 + \frac{1}{12} \left((6\omega + 6w_0 + 10w_a)\omega - w_a (e^\omega + 45e^{\omega/3} - 9e^{2\omega/3}) \right). \quad (23)$$

In Figs. 3, 4 and 5 the qualitative evolution of the scalar field equivalent $\phi(\omega)$, the scalar field potential $V(\omega)$ and the parametric plot $V(\omega)$ are presented respectively for the CPL parametrization (Ext1) and the other two extensions, namely, Ext2, and Ext3.

4. OBSERVATIONAL DATA

For the convenience of the reader and for our presentation we provide the details of the observational data used to constrain the dynamical dark energy parametrization and also the methodology.

- Cosmic microwave background observations: the cosmic microwave background (CMB) observations are one of the powerful data to probe the nature of dark energy. Here we use the CMB from Planck 2015 [47, 48]. The high- ℓ temperature and polarization data as well as the low- ℓ temperature and polarization data from Planck 2015 (precisely the dataset: Planck TT, TE, EE + lowTEB) [47, 48] have been considered.
- Baryon acoustic oscillations: The baryon acoustic oscillations (BAO) data from different superovulation missions are used [50–52].
- Supernovae Type Ia: We also use latest released Pantheon sample [53] from the Supernovae Type

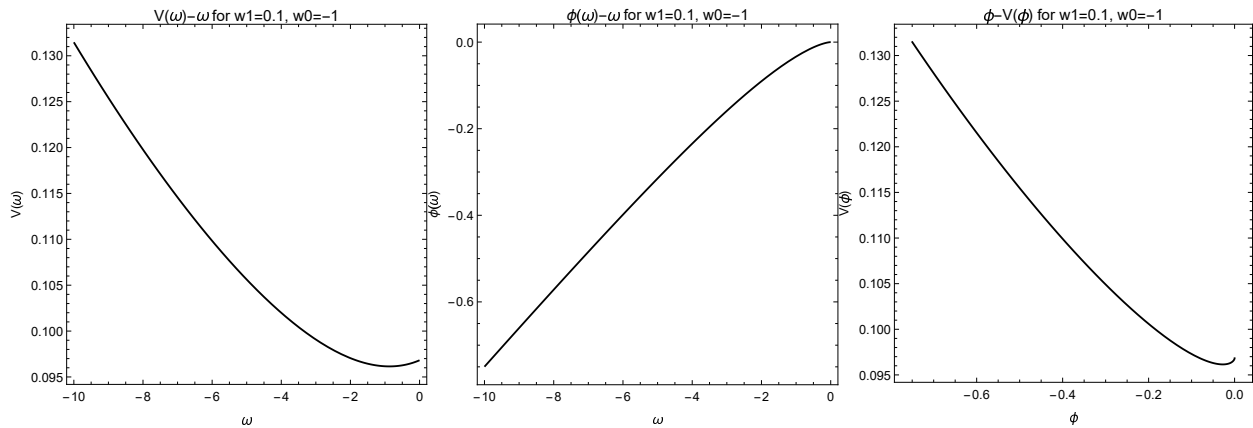


FIG. 3: Qualitative evolution of the scalar field $\phi(\omega)$, the scalar field potential $V(\omega)$ as also the parametric plot $\phi - V(\phi)$ is given for the CPL (Ext1) model.

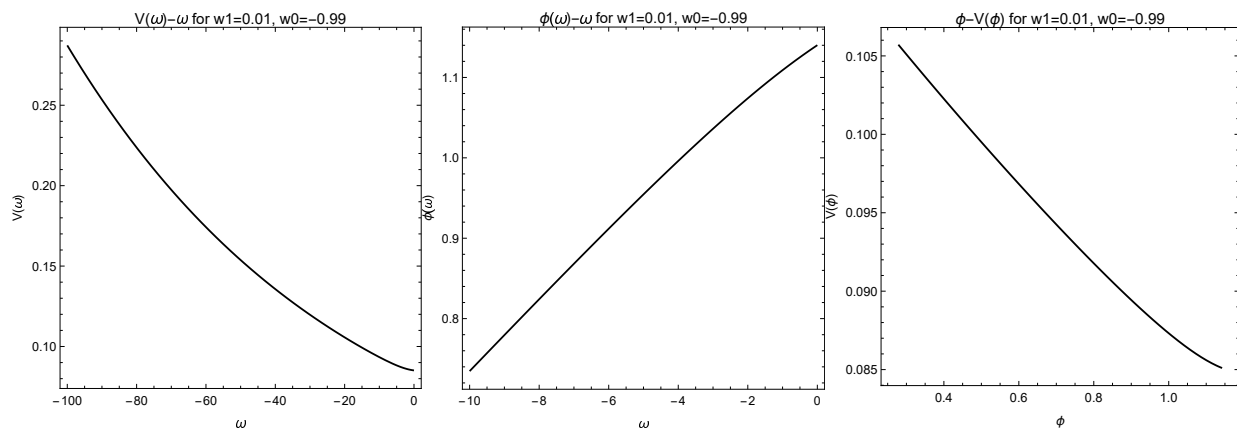


FIG. 4: Qualitative evolution of the scalar field $\phi(\omega)$, the scalar field potential $V(\omega)$ as also the parametric plot $\phi - V(\phi)$ is given for the Ext2 model.

Ia.

- Hubble parameter measurements: Finally, we use the Hubble parameter measurements from the Cosmic Chronometers (CC) [54].

Now we come to the technical part of the statistical analysis. Thus, we have performed the fitting analysis using the modified version of `cosmomc` [55, 56], an efficient markov chain monte carlo package equipped with a convergence diagnostic given by the Gelman and Rubin statistics [57]. This package includes the support for the Planck 2015 likelihood code [48] (see <http://cosmologist.info/cosmomc/>). In Table I we have shown the flat priors on the model parameters that have been used during the observational analysis. Perhaps it might be important to mention here that in the present analysis we have used Planck 2015 likelihood [48] instead of Planck 2018 likelihood (although the cosmological parameters from Planck 2018 are already available [58]) because Planck 2018 likelihood code is not public yet. However, it will be worth to run the same codes that we use for the present models but with the new Planck 2018

Parameter	Prior
$\Omega_b h^2$	[0.005, 0.1]
$\Omega_c h^2$	[0.01, 0.99]
τ	[0.01, 0.8]
n_s	[0.5, 1.5]
$\log[10^{10} A_s]$	[2.4, 4]
$100\theta_{MC}$	[0.5, 10]
w_0	[-2, 0]
w_a	[-3, 3]

TABLE I: The table shows the flat priors on the model parameters used during the statistical analysis.

likelihood which will enable us to understand any effective changes in the cosmological parameters and consequently more stringent constraints on them as well.

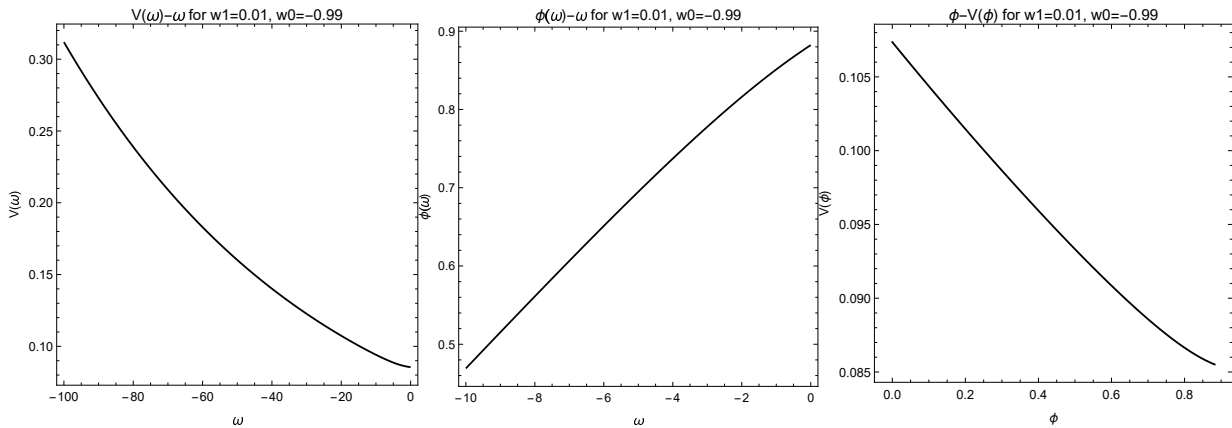


FIG. 5: Qualitative evolution of the scalar field $\phi(\omega)$, the scalar field potential $V(\omega)$ as also the parametric plot $\phi - V(\phi)$ is given for the Ext3 model.

Parameters	CMB+BAO	CMB+BAO+Pantheon	CMB+BAO+Pantheon+CC
$\Omega_c h^2$	$0.1194^{+0.0013+0.0027}_{-0.0014-0.0026}$	$0.1193^{+0.0013+0.0024}_{-0.0013-0.0025}$	$0.1195^{+0.0013+0.0026}_{-0.0013-0.0026}$
$\Omega_b h^2$	$0.02222^{+0.00015+0.00029}_{-0.00015-0.00030}$	$0.02223^{+0.00015+0.00029}_{-0.00015-0.00029}$	$0.02222^{+0.00014+0.00030}_{-0.00015-0.00030}$
$100\theta_{MC}$	$1.04049^{+0.00032+0.00063}_{-0.00032-0.00066}$	$1.04051^{+0.00030+0.00063}_{-0.00031-0.00062}$	$1.04049^{+0.00032+0.00063}_{-0.00032-0.00063}$
τ	$0.079^{+0.018+0.033}_{-0.018-0.035}$	$0.080^{+0.018+0.034}_{-0.017-0.034}$	$0.079^{+0.018+0.034}_{-0.018-0.034}$
n_s	$0.9738^{+0.0044+0.0086}_{-0.0044-0.0085}$	$0.9740^{+0.0041+0.0083}_{-0.0041-0.0082}$	$0.9735^{+0.0042+0.0080}_{-0.0042-0.0078}$
$\ln(10^{10} A_s)$	$3.100^{+0.035+0.064}_{-0.034-0.068}$	$3.103^{+0.034+0.066}_{-0.034-0.067}$	$3.101^{+0.034+0.066}_{-0.035-0.066}$
w_0	$-0.537^{+0.442+0.532}_{-0.441-0.526}$	$-0.963^{+0.060+0.158}_{-0.082-0.127}$	$-0.933^{+0.071+0.140}_{-0.070-0.135}$
w_a	$-1.154^{+0.894+1.340}_{-0.807-1.298}$	$-0.231^{+0.291+0.416}_{-0.143-0.499}$	$-0.337^{+0.288+0.431}_{-0.204-0.493}$
Ω_{m0}	$0.348^{+0.034+0.055}_{-0.035-0.056}$	$0.306^{+0.007+0.015}_{-0.007-0.014}$	$0.306^{+0.008+0.015}_{-0.008-0.015}$
σ_8	$0.804^{+0.026+0.056}_{-0.033-0.050}$	$0.839^{+0.018+0.031}_{-0.016-0.032}$	$0.840^{+0.016+0.033}_{-0.017-0.032}$
H_0	$64.14^{+2.51+5.60}_{-3.80-5.12}$	$68.24^{+0.78+1.56}_{-0.80-1.51}$	$68.23^{+0.84+1.67}_{-0.83-1.62}$

TABLE II: Observational constraints on various free parameters at 68% and 95% CL for the dynamical dark energy state parameter $w_x(z) = (w_0 - w_a) + w_a \exp\left(\frac{z}{1+z}\right)$ (Gen) using different astronomical datasets have been presented. Let us note that Ω_{m0} is the present value of $\Omega_m = \Omega_c + \Omega_b$ and H_0 is in the units of km/sec/Mpc.

5. OBSERVATIONAL CONSTRAINTS AND THE ANALYSIS

In this section we describe the observational constraints on all the dark energy parametrization, namely the general parametrization of eqn. (6), Extension 1 or the CPL parametrization of eqn. (7), Extension 2 of eqn. (8) and extension 3 of eqn. (9) using various astronomical datasets summarized in section 4. In particular, we focus on the two key parameters of the dark energy parametrization, namely, w_0 and w_a in order to investigate the qualitative changes in the parametrization as long as nonlinear terms are considered. In what follows we describe the observational constraints extracted from each dark energy scenario.

Let us first focus on the general dark energy parametrization given in equation (6). We have constrained this dark energy scenario using different cosmological datasets such as CMB+BAO, CMB+BAO+Pantheon and CMB+BAO+Pantheon+CC, the results of which are summarized in Table II. From Table II, a general conclusion that one might quickly observe is that, the inclusion of Pantheon to CMB+BAO significantly improves the error bars on all the parameters, and not only that, some of the parameters are significantly improved concerning their mean value. In fact, the best constraints on the model parameters are achieved for the combination CMB+BAO+Pantheon. The inclusion of CC to CMB+BAO+Pantheon although does not add much significant insight on the cosmological constraints, however, the effects on w_a are pronounced when CC data are added to CMB+BAO+Pantheon. Let us now focus on the constraints on individual model parameters. As one can see from Table II that the mean value of the dark energy equation of state at present, i.e., w_0 is always in the quintessential regime: $w_0 = -0.963^{+0.060}_{-0.082}$ at 68%

Parameters	CMB+BAO	CMB+BAO+Pantheon	CMB+BAO+Pantheon+CC
$\Omega_c h^2$	$0.1191^{+0.0014+0.0026}_{-0.0013-0.0027}$	$0.1191^{+0.0013+0.0025}_{-0.0013-0.0026}$	$0.1191^{+0.0013+0.0026}_{-0.0013-0.0026}$
$\Omega_b h^2$	$0.02226^{+0.00015+0.00029}_{-0.00015-0.00029}$	$0.02227^{+0.00015+0.00030}_{-0.00015-0.00030}$	$0.02227^{+0.00015+0.00030}_{-0.00015-0.00030}$
$100\theta_{MC}$	$1.04078^{+0.00033+0.00063}_{-0.00032-0.00064}$	$1.04080^{+0.00032+0.00064}_{-0.00031-0.00062}$	$1.04080^{+0.00031+0.00062}_{-0.00032-0.00062}$
τ	$0.078^{+0.017+0.034}_{-0.017-0.034}$	$0.080^{+0.017+0.035}_{-0.017-0.035}$	$0.080^{+0.018+0.034}_{-0.018-0.034}$
n_s	$0.9665^{+0.0044+0.0091}_{-0.0044-0.0084}$	$0.9667^{+0.0044+0.0089}_{-0.0044-0.0086}$	$0.9666^{+0.0045+0.0087}_{-0.0044-0.0087}$
$\ln(10^{10} A_s)$	$3.090^{+0.034+0.066}_{-0.033-0.066}$	$3.092^{+0.034+0.066}_{-0.033-0.068}$	$3.092^{+0.034+0.066}_{-0.034-0.066}$
w_0	$-0.524^{+0.374+0.524}_{-0.236-0.514}$	$-0.947^{+0.076+0.165}_{-0.088-0.156}$	$-0.950^{+0.075+0.152}_{-0.084-0.152}$
w_a	$-1.403^{+0.731+1.570}_{-1.021-1.466}$	$-0.308^{+0.367+0.619}_{-0.273-0.677}$	$-0.291^{+0.338+0.555}_{-0.256-0.588}$
Ω_{m0}	$0.344^{+0.032+0.051}_{-0.026-0.054}$	$0.304^{+0.008+0.016}_{-0.007-0.015}$	$0.304^{+0.008+0.015}_{-0.008-0.015}$
σ_8	$0.803^{+0.024+0.053}_{-0.030-0.051}$	$0.838^{+0.018+0.032}_{-0.016-0.033}$	$0.837^{+0.016+0.032}_{-0.016-0.032}$
H_0	$64.36^{+2.05+5.26}_{-3.23-4.67}$	$68.34^{+0.81+1.70}_{-0.82-1.63}$	$68.31^{+0.84+1.64}_{-0.83-1.66}$

TABLE III: Observational constraints on the dark energy parametrization, namely, the Ext1 of (7) using various observational datasets. We note that H_0 is in the units of km/Mpc/sec and Ω_{m0} is the present value of $\Omega_m = \Omega_b + \Omega_c$.

Parameters	CMB+BAO	CMB+BAO+Pantheon	CMB+BAO+Pantheon+CC
$\Omega_c h^2$	$0.1192^{+0.0014+0.0026}_{-0.0013-0.0027}$	$0.1194^{+0.0013+0.0026}_{-0.0013-0.0025}$	$0.1195^{+0.0013+0.0027}_{-0.0014-0.0027}$
$\Omega_b h^2$	$0.02223^{+0.00015+0.00030}_{-0.00015-0.00030}$	$0.02223^{+0.00015+0.00028}_{-0.00015-0.00028}$	$0.02222^{+0.00015+0.00028}_{-0.00015-0.00029}$
$100\theta_{MC}$	$1.04051^{+0.00032+0.00064}_{-0.00034-0.00063}$	$1.04051^{+0.00031+0.00061}_{-0.00033-0.00059}$	$1.04050^{+0.00033+0.00062}_{-0.00033-0.00065}$
τ	$0.079^{+0.018+0.034}_{-0.018-0.035}$	$0.079^{+0.017+0.033}_{-0.017-0.035}$	$0.081^{+0.017+0.036}_{-0.018-0.035}$
n_s	$0.9744^{+0.0043+0.0083}_{-0.0043-0.0088}$	$0.9740^{+0.0042+0.0086}_{-0.0045-0.0082}$	$0.9740^{+0.0045+0.0085}_{-0.0043-0.0086}$
$\ln(10^{10} A_s)$	$3.100^{+0.035+0.067}_{-0.035-0.068}$	$3.100^{+0.036+0.064}_{-0.033-0.067}$	$3.104^{+0.034+0.069}_{-0.034-0.070}$
w_0	$-0.616^{+0.326+0.560}_{-0.428-0.501}$	$-0.949^{+0.074+0.149}_{-0.076-0.139}$	$-0.946^{+0.072+0.155}_{-0.088-0.150}$
w_a	$-1.000^{+1.039+1.262}_{-0.609-1.427}$	$-0.290^{+0.277+0.460}_{-0.217-0.534}$	$-0.302^{+0.310+0.500}_{-0.219-0.533}$
Ω_{m0}	$0.339^{+0.031+0.058}_{-0.037-0.054}$	$0.305^{+0.008+0.015}_{-0.008-0.015}$	$0.306^{+0.008+0.015}_{-0.007-0.015}$
σ_8	$0.810^{+0.030+0.055}_{-0.032-0.053}$	$0.839^{+0.016+0.031}_{-0.016-0.031}$	$0.841^{+0.016+0.033}_{-0.016-0.033}$
H_0	$64.98^{+3.11+5.55}_{-3.35-5.47}$	$68.29^{+0.81+1.65}_{-0.82-1.59}$	$68.24^{+0.79+1.56}_{-0.82-1.50}$

TABLE IV: Observational constraints on the dark energy parametrization, namely, the Ext2 of (8) using various observational datasets. We note that H_0 is in the units of km/Mpc/sec and Ω_{m0} is the present value of $\Omega_m = \Omega_b + \Omega_c$.

Parameters	CMB+BAO	CMB+BAO+Pantheon	CMB+BAO+Pantheon+CC
$\Omega_c h^2$	$0.1195^{+0.0013+0.0027}_{-0.0013-0.0027}$	$0.1194^{+0.0013+0.0026}_{-0.0013-0.0027}$	$0.1195^{+0.0013+0.0027}_{-0.0013-0.0025}$
$\Omega_b h^2$	$0.02222^{+0.00014+0.00029}_{-0.00014-0.00029}$	$0.02222^{+0.00015+0.00030}_{-0.00014-0.00029}$	$0.02221^{+0.00015+0.00029}_{-0.00015-0.00029}$
$100\theta_{MC}$	$1.04049^{+0.00031+0.00065}_{-0.00032-0.00065}$	$1.04050^{+0.00033+0.00062}_{-0.00032-0.00065}$	$1.04047^{+0.00032+0.00061}_{-0.00032-0.00063}$
τ	$0.078^{+0.018+0.035}_{-0.018-0.036}$	$0.080^{+0.018+0.034}_{-0.017-0.035}$	$0.079^{+0.018+0.033}_{-0.017-0.034}$
n_s	$0.9737^{+0.0043+0.0089}_{-0.0043-0.0083}$	$0.9738^{+0.0043+0.0086}_{-0.0043-0.0086}$	$0.9737^{+0.0043+0.0084}_{-0.0043-0.0084}$
$\ln(10^{10} A_s)$	$3.099^{+0.035+0.067}_{-0.036-0.069}$	$3.104^{+0.034+0.066}_{-0.033-0.067}$	$3.101^{+0.034+0.065}_{-0.034-0.067}$
w_0	$-0.582^{+0.490+0.581}_{-0.501-0.564}$	$-0.946^{+0.070+0.147}_{-0.080-0.137}$	$-0.936^{+0.072+0.138}_{-0.071-0.141}$
w_a	$-1.077^{+1.176+1.422}_{-1.010-1.450}$	$-0.295^{+0.284+0.483}_{-0.215-0.508}$	$-0.335^{+0.264+0.471}_{-0.222-0.472}$
Ω_{m0}	$0.343^{+0.042+0.058}_{-0.045-0.059}$	$0.306^{+0.0075+0.015}_{-0.0075-0.015}$	$0.306^{+0.0076+0.016}_{-0.0083-0.015}$
σ_8	$0.808^{+0.028+0.059}_{-0.036-0.052}$	$0.840^{+0.016+0.031}_{-0.016-0.031}$	$0.841^{+0.016+0.032}_{-0.017-0.034}$
H_0	$64.67^{+3.73+6.18}_{-4.37-5.42}$	$68.26^{+0.80+1.57}_{-0.82-1.58}$	$68.27^{+0.83+1.73}_{-0.85-1.62}$

TABLE V: Observational constraints on the dark energy parametrization, namely, the Ext3 of (9) using various observational datasets. We note that H_0 is in the units of km/Mpc/sec and Ω_{m0} is the present value of $\Omega_m = \Omega_b + \Omega_c$.

Datasets	Parameters	Gen	Ext1 (CPL)	Ext2	Ext3
CB	(w_0, w_a)	$(-0.537^{+0.442}_{-0.441}, -1.154^{+0.894}_{-0.807})$	$(-0.524^{+0.374}_{-0.236}, -1.403^{+0.731}_{-1.021})$	$(-0.616^{+0.326}_{-0.428}, -1.000^{+1.039}_{-0.609})$	$(-0.582^{+0.490}_{-0.501}, -1.077^{+1.176}_{-1.010})$
CBP	(w_0, w_a)	$(-0.963^{+0.060}_{-0.082}, -0.231^{+0.291}_{-0.143})$	$(-0.947^{+0.076}_{-0.088}, -0.308^{+0.367}_{-0.273})$	$(-0.949^{+0.074}_{-0.076}, -0.290^{+0.277}_{-0.215})$	$(-0.946^{+0.070}_{-0.080}, -0.295^{+0.284}_{-0.215})$
CMPC	(w_0, w_a)	$(-0.933^{+0.071}_{-0.070}, -0.337^{+0.288}_{-0.204})$	$(-0.950^{+0.075}_{-0.084}, -0.291^{+0.338}_{-0.256})$	$(-0.946^{+0.072}_{-0.088}, -0.302^{+0.310}_{-0.219})$	$(-0.936^{+0.072}_{-0.071}, -0.335^{+0.264}_{-0.222})$

TABLE VI: For a clear understandig and comparison of the dark energy key parameters (w_0, w_a) extracted from all the parametrizations, we show their estimations at 68% CL. Here, CB = CMB+BAO, CBP = CMB+BAO+Pantheon, CBPC = CMB+BAO+Pantheon+CC.

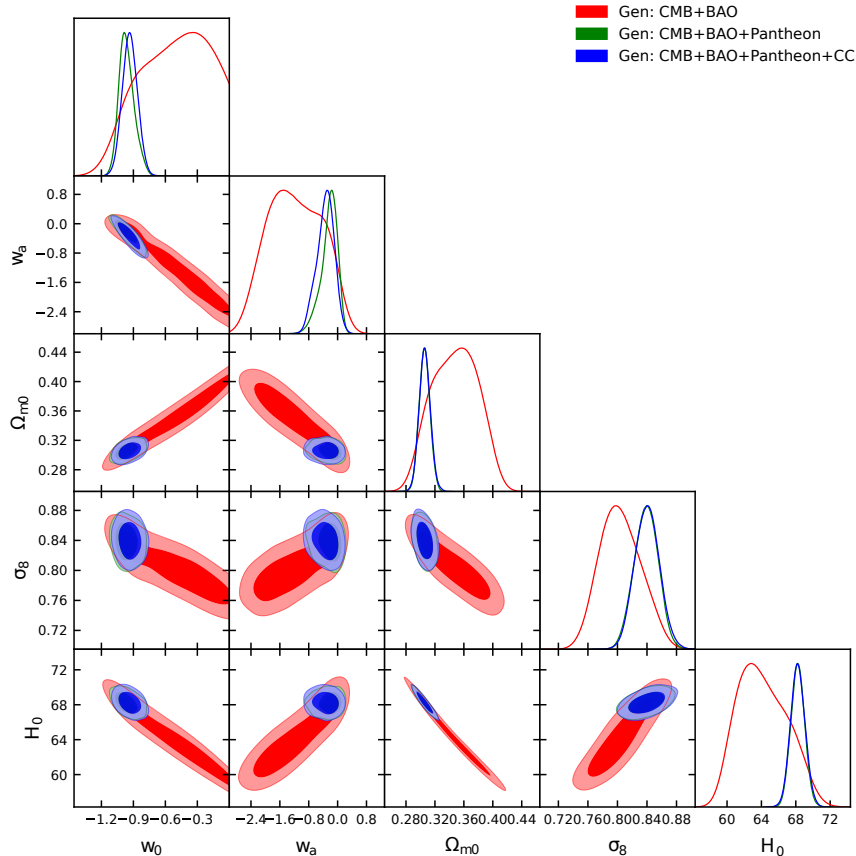


FIG. 6: 68% and 95% CL contour plots for various combinations of the model parameters of the general parametrization of (6) (Gen) have been shown for different observational combinations. The figure also contains the one dimensional marginalized posterior distributions for the parameters shown in the two dimensional contour plots.

CL for CMB+BAO+Pantheon and $w_0 = -0.933^{+0.071}_{-0.070}$ at 68% CL for CMB+BAO+Pantheon+CC. Although from statistical point of view, one can argue that the constraints on w_0 mildly suggest for a crossing of the phantom divide line $w_0 = -1$, however, $w_0 = -1$ is the most consistent scenario. Concerning the remaining key parameter, w_a , we find that it may assume nonnull values, however, $w_a = 0$ is allowed within 68% CL of course. In Fig. 6, we have shown the one dimensional posterior distributions for some selected parameters of this model as well as the two dimensional contour plots considering various combinations of the model parameters. From Fig. 6, one can see that the parameters shown in this figure are correlated with each other. Specifically, we find a strong correlation between w_0 , w_a and H_0 . Finally, we focus on the estimation of the Hubble constant H_0 for all three datasets. One can strikingly see that for CMB+BAO, H_0 assumes a very lower value ($H_0 = 64.14^{+2.51}_{-3.80}$ at 68% CL, CMB+BAO) compared to the Λ CDM based Planck's estimation [59] and this naturally increases the tension with the local measurements [60]. However, for the remaining datasets, we find that H_0 takes higher values with slightly higher error bars compared to the Λ CDM based Planck's

estimation [59], thus, it slightly decreases the tension on it.

We now consider the first extension of the general parametrization (6) that leads to the well known CPL parametrization of (7). The cosmic scenario driven by this parametrization has been constrained using the same observational datasets applied to the general DE parametrization and the numerical results are summarized in Table III. One can clearly see that the Hubble constant takes similar values compared to the previous scenario (see Table II). In fact, concerning the key parameters, namely, w_0 and w_a , our conclusion remains same, that means the constraints on w_0 and w_a are almost similar to what we have found with the general parametrization (6). So, effectively we see that the first approximation (7) of the original parametrization (6) returns similar fit to the original parametrization (6). Finally, in Fig. 7 we have shown the graphical behaviour of various model parameters containing the one dimensional marginalized posterior distributions as well as the two dimensional contour plots at 68% and 95% CL.

Then we move to the observational constraints of the next parametrization given in eqn. 8. The results for this parametrization are shown in Table IV and Fig. 8. We

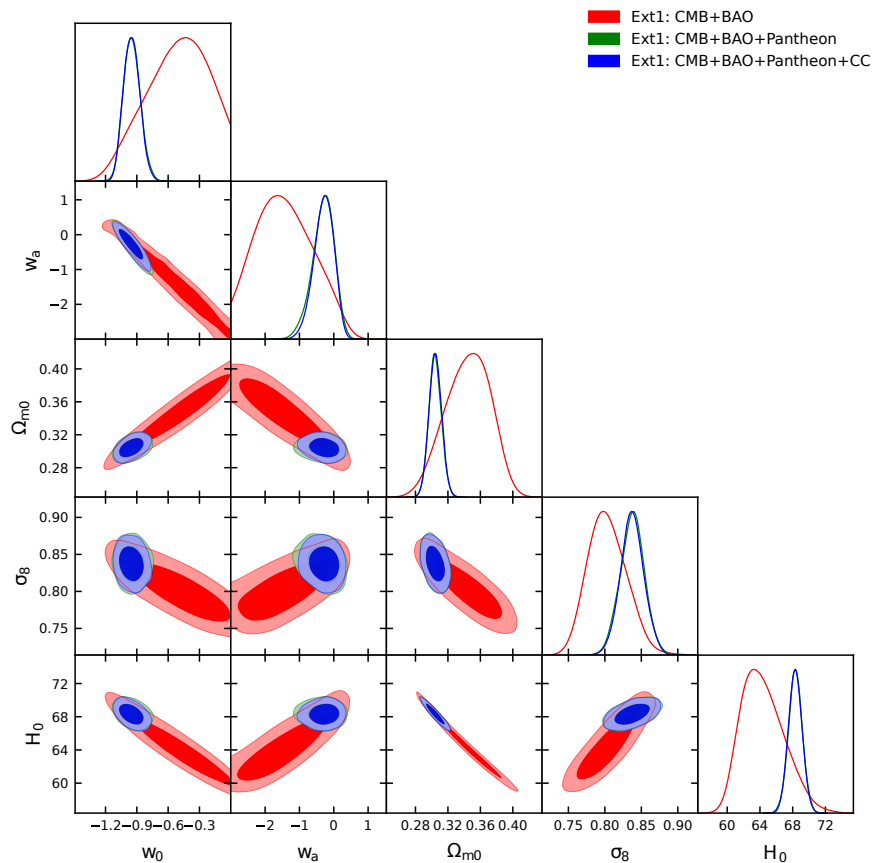


FIG. 7: 68% and 95% CL contour plots for various combinations of the model parameters of Ext1 of (7) [the CPL parametrization] have been shown for different observational combinations. The figure also contains the one dimensional marginalized posterior distributions for the parameters shown in the two dimensional contour plots.

do not find any notable changes due to the extension of one more term in the DE parametrization. That means, the parametrization behaves similarly to the previous two parametrizations.

Finally, we focus on the last parametrization of this series, namely Ext3 shown in eqn. (9). We have summarized the results in Table V and Fig. 9, using the same combinations of the cosmological datasets that have been used for the previous parametrizations. It is interesting to note that even if we successively increase the terms in the Taylor expansion of the generalized parametrization (6), but that does not attribute to any change in the constraints on the key parameters as well as on the derived parameters, for instance the Hubble constant. For a better understanding on the key parameters (w_0, w_a) obtained from various combined datasets, in Table VI, we have presented their 68% CL constraints and in Fig. 10, we have shown their two dimensional contour plots. The Table VI and Fig. 10 clearly emphasize that at the background level, none of the extensions can be distinguished from the general parametrization. However, as we will show below that, at the level of perturbations, the inclusion of higher order terms certainly exhibits some changes.

Thus, we investigate how the present dark energy parametrization, namely, the new dark energy parametrization in eqn. (6), and its extensions in equations (7), (8) and (9) affect various observables, such as the temperature anisotropy in the cosmic microwave background spectra as well as the matter power spectra. Such an investigation is important since this enables one to understand how the higher order extensions of the original dark energy parametrization (6) affect the structure formation of the universe. Thus, in Fig. 11 we show the temperature anisotropy in the CMB spectra and the residual plots for different dark energy parametrizations for various values of w_a parameter with a fixed value of $w_0 = -0.95$. We have actually fixed $w_0 = -0.95$ since from the observational analyses of the models presented in various tables of this article, w_0 assumes values close to -0.95 . For completeness, we have considered both the possibilities namely $w_a > 0$ and $w_a < 0$. The plots in the first row of Fig. 11 depict the temperature anisotropy in the CMB spectra for $w_a > 0$ and the plots in the second row of Fig. 11 describe the corresponding residual plots. Let us note that the plots from left to right in both the first and second rows of Fig. 11 respectively stand for $w_a = 0.1, 0.2, \text{ and } 0.3$. In a similar fashion, the plots

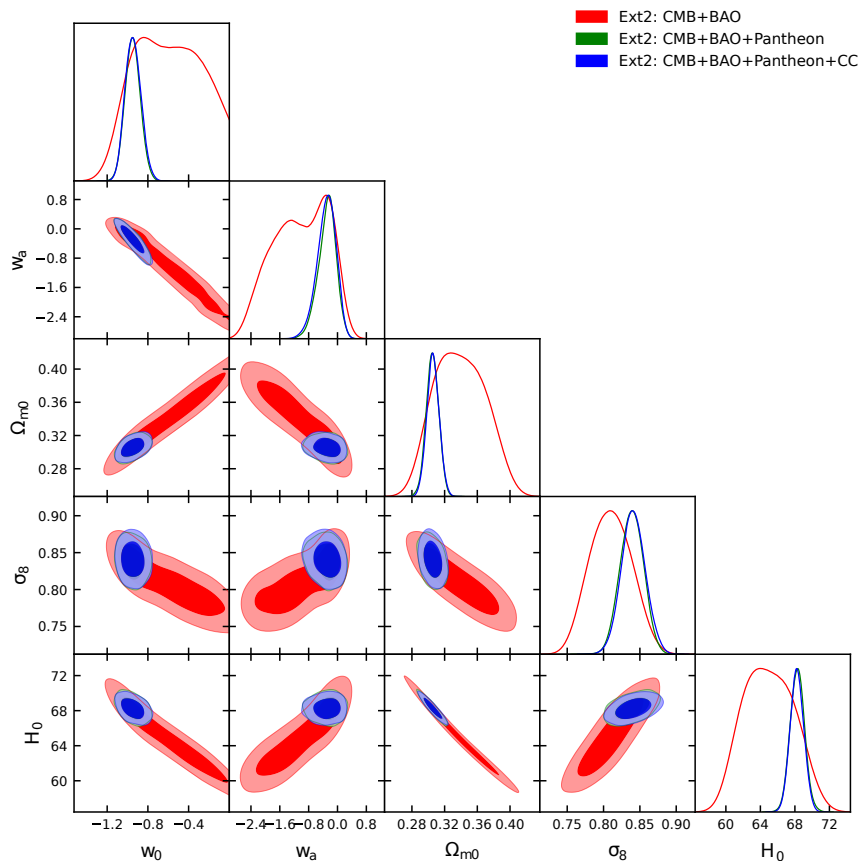


FIG. 8: 68% and 95% CL contour plots for various combinations of the model parameters of the Ext2 of (8) have been shown for different observational combinations. The figure also contains the one dimensional marginalized posterior distributions for the parameters shown in the two dimensional contour plots.

in the third row of Fig. 11 stands for the CMB spectra assuming $w_a < 0$ and the plots in the last row of Fig. 11 represent the corresponding residual plots. And the plots from left to right in both the third and last rows of Fig. 11 respectively stand for $w_a = -0.1, -0.2$ and -0.3 . From the first row of Fig. 11 one can clearly notice that the DE parametrizations cannot be distinguished from one another, even if we increase the magnitude of w_a , however, when we look at the corresponding residual plots shown in the second row of Fig. 11, we realize the differences. It is clear that that Ext3 is more close to the original parametrization (6) compared to Ext1 and Ext2. The same conclusion can be drawn from the last row of Fig. Fig. 11. So, effectively, independently of the sign of w_a , the conclusion remains same.

Following a similar graphical strategy applied to matter power spectra plots as shown in Fig. 12, we arrive at the same conclusion that the models are only distinguished from one another if we look at the residual plots, that means the plots summarized in the second and last rows of Fig. 12.

$\ln B_{ij}$	Evidence for model M_i
$0 \leq \ln B_{ij} < 1$	Weak
$1 \leq \ln B_{ij} < 3$	Definite/Positive
$3 \leq \ln B_{ij} < 5$	Strong
$\ln B_{ij} \geq 5$	Very strong

TABLE VII: Revised Jeffreys scale quantifying the observational viability of any cosmological model M_i compared to some reference model M_j [63].

6. BAYESIAN EVIDENCE

A general and natural question that we will be looking for in this section is that, how the models are efficient compared to the standard Λ CDM cosmology. Thus, we need a statistical comparison between all four dynamical DE parametrizations where the base model will be fixed as Λ CDM. This statistical comparison comes through the Bayesian evidence. Here we apply publicly available code

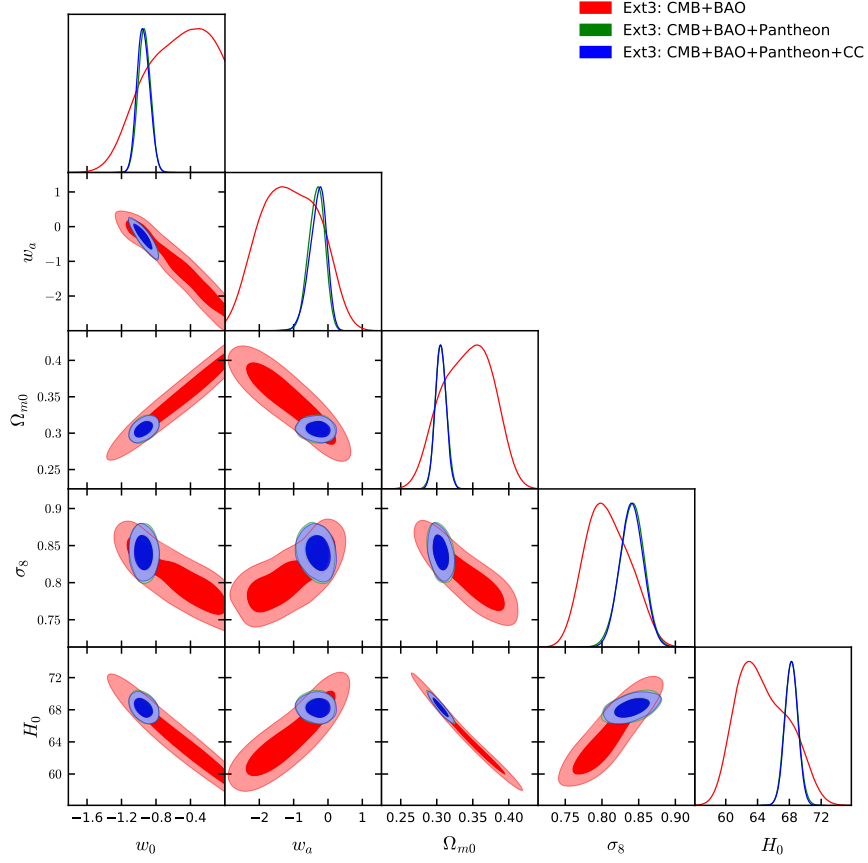


FIG. 9: 68% and 95% CL contour plots for various combinations of the model parameters of the Ext3 of (9) have been shown for different observational combinations. The figure also contains the one dimensional marginalized posterior distributions for the parameters shown in the two dimensional contour plots.

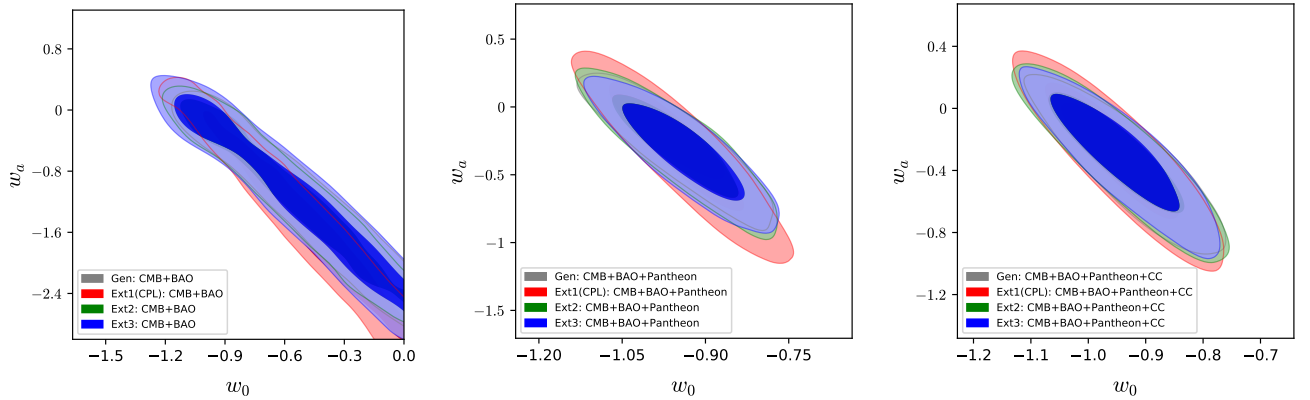


FIG. 10: We show the (w_0, w_a) plane for the present dynamical dark energy parametrizations using different observational datasets. The left graph for the dataset CMB+BAO, the middle graph for the dataset CMB+BAO+Pantheon and the right graph stands for the observational dataset CMB+BAO+Pantheon+CC.

MCEvidence [61, 62]¹ to compute the evidences of the

models. The use of MCEvidence is very easy since the code only needs the MCMC chains used to extract the free parameters of the DE parametrizations.

While dealing with Bayesian analysis we need the posterior probability of the model parameters (denoted by

¹ See github.com/yabebalFantaye/MCEvidence.

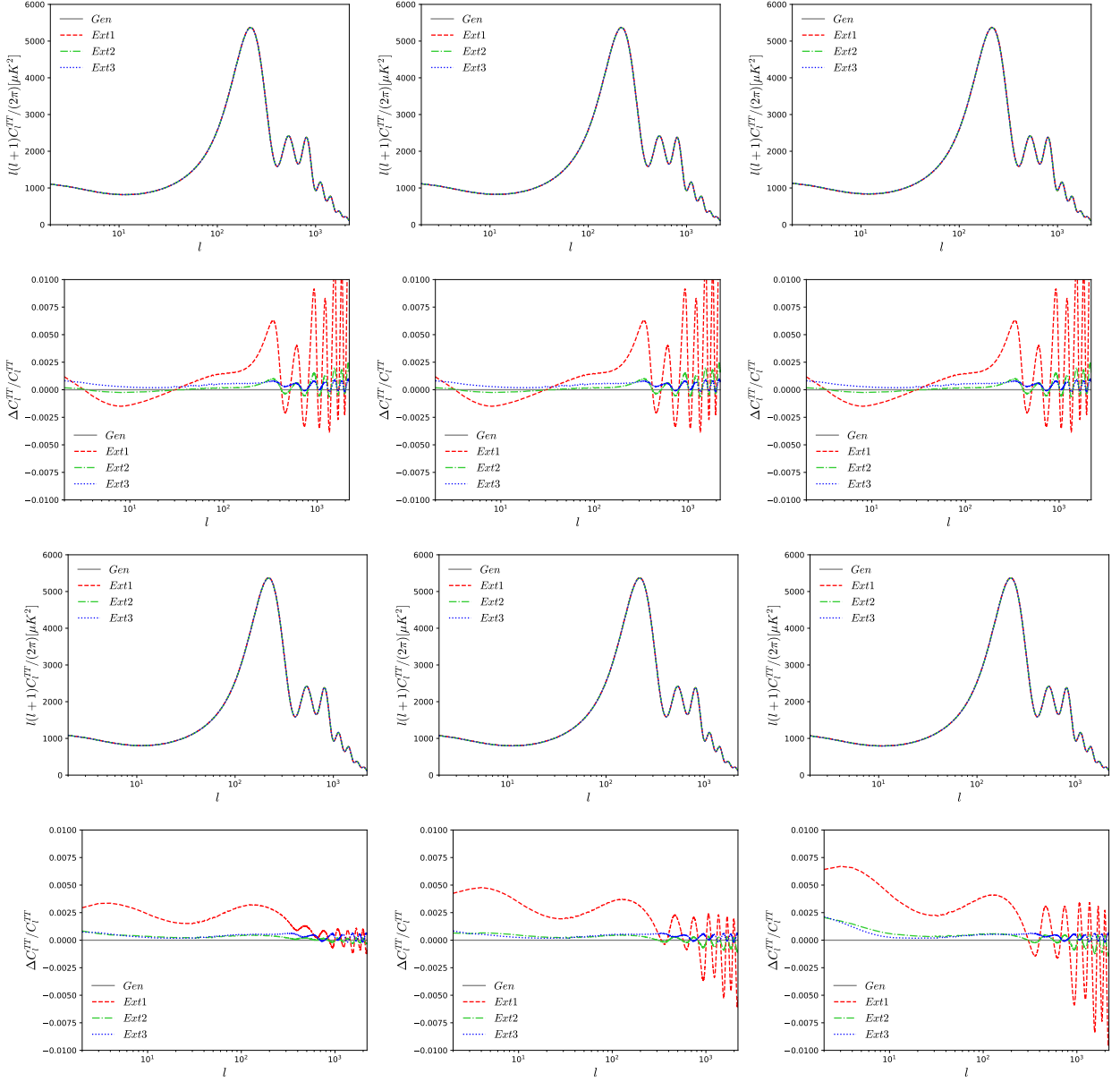


FIG. 11: We show the cosmic microwave background spectra and the corresponding residual plots for the present dynamical dark energy parameterizations using various values of the w_a parameter with a fixed $w_0 = -0.95$. The plots in the first row present the cosmic microwave background spectra and the plots in the second row present the corresponding residual plots. The plots from left to right in the first and second panels of this figure respectively stand for $w_a = 0.1, 0.2$, and 0.3 . Similarly, the plots in the third row (showing the cosmic microwave background spectra) and last row (residual plots of the third row) stand for $w_a < 0$ in which the plots from left to right for both the above rows (third and last rows) of this figure respectively stand for $w_a = -0.1, -0.2$, and -0.3 .

θ), given a specific observational data (x) with any prior information for a model (M). Following Bayes theorem, one can write,

$$p(\theta|x, M) = \frac{p(x|\theta, M) \pi(\theta|M)}{p(x|M)}, \quad (24)$$

where $p(x|\theta, M)$ is the likelihood as a function of θ and $\pi(\theta|M)$ refers to the prior information. Here, the quantity $p(x|M)$ appearing in the denominator of (24) is the

Bayesian evidence that we actually need for the model comparison. Now, for two cosmological models M_i, M_j where M_j is acting as the reference model², the posterior

² The reference model should be the most well motivated cosmological model that must be highly sound to the observational data; and without any doubt, Λ CDM is the best choice for such

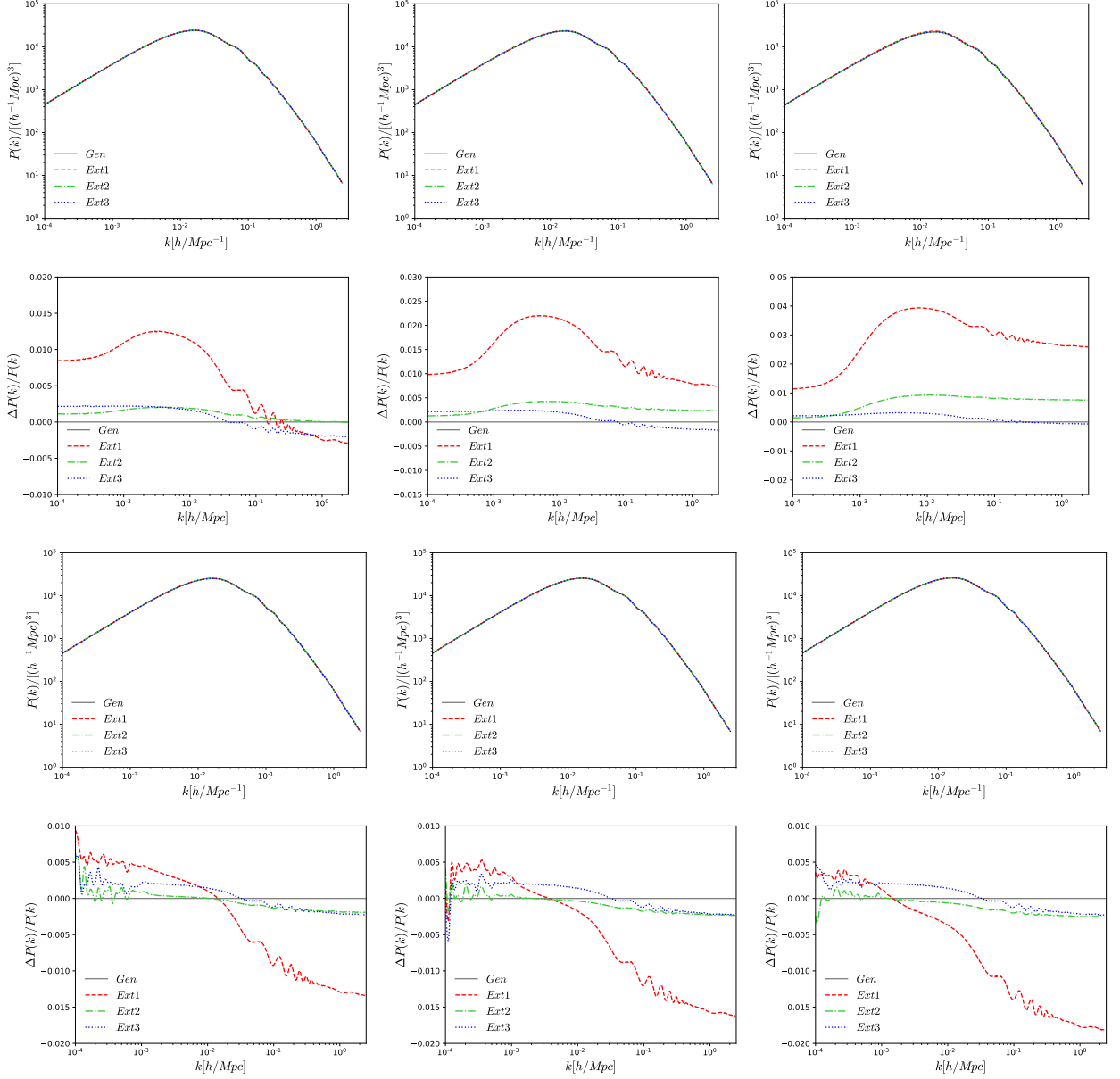


FIG. 12: We show the matter power spectra and the corresponding residual plots for the present dynamical dark energy parameterizations using various values of the w_a parameter with a fixed $w_0 = -0.95$. The plots in the first row present the matter power spectra and the plots in the second row present the corresponding residual plots. The plots from left to right in the first and second panels of this figure respectively stand for $w_a = 0.1, 0.2$, and 0.3 . Similarly, the plots in the third row (showing the matter power spectra) and last row (residual plots of the third row) stand for $w_a < 0$ in which the plots from left to right for both the above rows (third and last rows) of this figure respectively stand for $w_a = -0.1, -0.2$, and -0.3 .

probability is,

$$\frac{p(M_i|x)}{p(M_j|x)} = \frac{\pi(M_i)}{\pi(M_j)} \frac{p(x|M_i)}{p(x|M_j)} = \frac{\pi(M_i)}{\pi(M_j)} B_{ij}, \quad (25)$$

in which $B_{ij} = \frac{p(x|M_i)}{p(x|M_j)}$, is the Bayes factor of the model M_i relative to M_j . And based on the values of B_{ij} (alternatively, $\ln B_{ij}$) we quantify the observational support of the underlying model M_i relative to M_j . The quantification is done through the widely accepted Jeffreys scales [63] (see Table VII). We also note that the negative values of $\ln B_{ij}$ indicate that the reference model (M_j) is preferred over the underlying model (M_i).

a model comparison.

In Table VIII we have shown the values of $\ln B_{ij}$ com-

Dataset	Model	$\ln B_{ij}$	Evidence for Λ CDM
CMB+BAO	Gen	-1.4	Definite
CMB+BAO+Pantheon	Gen	-3.4	Strong
CMB+BAO+Pantheon+CC	Gen	-3.6	Strong
CMB+BAO	Ext1	-1.1	Definite
CMB+BAO+Pantheon	Ext1	-3.3	Strong
CMB+BAO+Pantheon+CC	Ext1	-3.4	Strong
CMB+BAO	Ext2	-1.7	Definite
CMB+BAO+Pantheon	Ext2	-3.2	Strong
CMB+BAO+Pantheon+CC	Ext2	-3.3	Strong
CMB+BAO	Ext3	-1.6	Definite
CMB+BAO+Pantheon	Ext3	-3.9	Strong
CMB+BAO+Pantheon+CC	Ext3	-3.5	Strong

TABLE VIII: The values of $\ln B_{ij}$ computed for the present dark energy parametrizations (M_i) where the reference scenario is the Λ CDM model (M_j). We note that the negative value of $\ln B_{ij}$ means that Λ CDM is preferred.

puted for all DE parametrizations considering all the datasets. We find that the values of $\ln B_{ij}$ are all negative indicating that Λ CDM is always preferred and this is true for all the observational datasets.

7. CONCLUDING REMARKS

The dark energy, a hypothetical fluid in Einstein gravity is the main concern of this work. This dark energy, as examined by many investigators since the year 1998, could be anything obeying only one condition that the pressure of the fluid should be negative. Thereafter, a cluster of dark energy models have been introduced and confronted with the observational data, see [1] to get an overview of the models.

Among them an interesting construction of the dark energy models comes through the equation of state of dark energy, $w_x = p_x/\rho_x$ which in principle is the function of the underlying cosmological time parameter, usually the function of the redshift. Technically, there is no such restriction to pick up any specific functional form for w_x , however, the viability of the model is only tested through the observational data and its effects on the large scale structure of the universe indeed. According to the investigations performed in the last couple of years, the Chevallier-Polarski-Linder parametrization is a feasible and well functioning dark energy parametrization with the observational data. The present work is motivated in the same direction whilst we have investigated something different as follows.

We have introduced a new dark energy parametrization (6) having a novel feature. The model recovers the well known CPL parametrization in its first order Taylor series expansion around $z = 0$. Thus, the model actually presents a generalized version of the CPL parametrization. Since the model is a nonlinear generalized version of the CPL model, thus, a natural inquiry one may ask for is, how its higher order corrections are important for the expansion history of the universe, and moreover, how the

higher order corrections could affect the evolution of the universe at the level of background and perturbations. In order to investigate these issues, we have considered the generalized model (6) together with its first, second and third order Taylor approximations around the present cosmic epoch $z = 0$, given in equations (7), (8) and (9). Since the original model (6) contains only two free parameters w_0 (current value of the dark energy equation of state) and w_a (parameter quantifying the dynamical nature of the DE), thus its extensions contain the same free parameters. We then constrain all the models using a class of astronomical data, such as CMB, BAO, Pantheon from SNIa and the Hubble parameter measurements (summarized in section 4).

The observational constraints are summarized in Table II (for eqn. (6)), Table III (for eqn. (7)), Table IV (for eqn. (8)), Table V (for eqn. (9)) and the graphical variations of the model parameters are also shown in Fig. 6, Fig. 7, Fig. 8 and Fig. 9, respectively for the general, Ext1, Ext2, and Ext3 parametrizations. From the analyses, it is clear that the cosmological parameters assume similar constraints and according to the employed observational data applied to the present models, the dark energy equation of state at present, w_0 , is consistent to $w_0 = -1$ scenario. In addition, we find that, for CMB+BAO data, H_0 for all parametrizations, assumes very lower values, if we disregard its error bars, however, for CMB+BAO+Pantheon and CMB+BAO+Pantheon+CC, H_0 increases with slightly higher error bars compared to the Λ CDM based Planck's estimation [59], and as a result the tension on H_0 is slightly reduced. However, at the level of background, the models cannot be distinguished from one another while from the investigations at perturbations stage, one can distinguish between the models, see the residual plots in Fig. 11 and Fig. 12.

We also performed the Bayesian evidence analysis using the `MCEvidence` and compared the models with respect to the standard Λ CDM reference scenario. Our analysis reveals that Λ CDM is favored over all the dy-

namical DE parametrizations. This is an expected result because the parameters space of the leading cosmic scenarios driven by the present dynamical DE parametrizations are of eight dimensional while Λ CDM has only six parameters.

Last but not least, we would like to comment that the model (6), so far we are aware of the literature, is a new one in the field of dark energy which naturally recovers CPL parametrization in its first order approximation and sounds good with the Bayesian evidence. Therefore, a number of investigations can be performed in various contexts of current interests. A quite straightforward and appealing investigation would be to measure the mass bounds of neutrinos in such a generalized framework. Moreover, it will be further interesting to consider a number of upcoming cosmological surveys, such as, Simons Observatory Collaboration (SOC) [64], Cosmic Microwave Background Stage-4 (CMB-S4) [65], EUCLID Collaboration [66, 67], Dark Energy Spectroscopic Instrument (DESI) [68], Large Synoptic Survey Telescope (LSST) [69–71], in order to forecast the present

dark energy parametrizations. The inclusion of gravitational waves data from various sources, such as, Laser Interferometer Space Antenna (LISA) [72], Deci-hertz Interferometer Gravitational wave Observatory (DECIGO) [73, 74], TianQin [75], is also an appealing direction of research in this direction.

Acknowledgments

The authors thank the referee for some useful and important comments that helped to improve the quality of the manuscript. SP acknowledges the financial support through the Faculty Research and Professional Development Fund (FRPDF) Scheme of Presidency University, Kolkata, India. WY was supported by the financial support from the National Natural Science Foundation of China under Grants No. 11705079 and No. 11647153. AP acknowledges financial support of FONDECYT grant no. 3160121.

-
- [1] E. J. Copeland, M. Sami and S. Tsujikawa, *Dynamics of dark energy*, Int. J. Mod. Phys. D **15**, 1753 (2006).
 - [2] M. Chevallier and D. Polarski, *Accelerating universes with scaling dark matter*, Int. J. Mod. Phys. D **10**, 213 (2001).
 - [3] E. V. Linder, *Exploring the expansion history of the universe*, Phys. Rev. Lett. **90**, 091301 (2003).
 - [4] A. R. Cooray and D. Huterer, *Gravitational lensing as a probe of quintessence*, Astrophys. J. **513**, L95 (1999).
 - [5] G. Efstathiou, *Constraining the equation of state of the universe from distant type Ia supernovae and cosmic microwave background anisotropies*, Mon. Not. Roy. Astron. Soc. **310**, 842 (1999).
 - [6] P. Astier, *Can luminosity distance measurements probe the equation of state of dark energy*, Phys. Lett. B **500**, 8 (2001).
 - [7] J. Weller and A. Albrecht, *Future supernovae observations as a probe of dark energy*, Phys. Rev. D **65**, 103512 (2002).
 - [8] C. Wetterich, *Phenomenological parameterization of quintessence*, Phys. Lett. B **594**, 17 (2004).
 - [9] S. Hannestad and E. Mortsell, *Cosmological constraints on the dark energy equation of state and its evolution*, JCAP **0409**, 001 (2004).
 - [10] H. K. Jassal, J. S. Bagla and T. Padmanabhan, *Observational constraints on low redshift evolution of dark energy: How consistent are different observations?*, Phys. Rev. D **72**, 103503 (2005).
 - [11] Y. g. Gong and Y. Z. Zhang, *Probing the curvature and dark energy*, Phys. Rev. D **72**, 043518 (2005).
 - [12] B. Feng, M. Li, Y. S. Piao and X. Zhang, *Oscillating quintom and the recurrent universe*, Phys. Lett. B **634**, 101 (2006).
 - [13] S. Nojiri and S. D. Odintsov, *The Oscillating dark energy: Future singularity and coincidence problem*, Phys. Lett. B **637**, 139 (2006).
 - [14] G. B. Zhao, J. Q. Xia, H. Li, C. Tao, J. M. Virey, Z. H. Zhu and X. Zhang, *Probing for dynamics of dark energy and curvature of universe with latest cosmological observations*, Phys. Lett. B **648**, 8 (2007).
 - [15] A. Kurek, O. Hrycyna and M. Szydlowski, *Constraints on oscillating dark energy models*, Phys. Lett. B **659**, 14 (2008).
 - [16] E. M. Barboza, Jr. and J. S. Alcaniz, *A parametric model for dark energy*, Phys. Lett. B **666**, 415 (2008).
 - [17] E. N. Saridakis, *Theoretical Limits on the Equation-of-State Parameter of Phantom Cosmology*, Phys. Lett. B **676**, 7 (2009).
 - [18] R. Lazkoz, V. Salzano and I. Sendra, *Oscillations in the dark energy EoS: new MCMC lessons*, Phys. Lett. B **694**, 198 (2010).
 - [19] J. Z. Ma and X. Zhang, *Probing the dynamics of dark energy with novel parametrizations*, Phys. Lett. B **699**, 233 (2011).
 - [20] H. Li and X. Zhang, *Probing the dynamics of dark energy with divergence-free parametrizations: A global fit study*, Phys. Lett. B **703**, 119 (2011).
 - [21] L. Feng and T. Lu, *A new equation of state for dark energy model*, JCAP **1111**, 034 (2011).
 - [22] I. Sendra and R. Lazkoz, *SN and BAO constraints on (new) polynomial dark energy parametrizations: current results and forecasts*, Mon. Not. Roy. Astron. Soc. **422**, 776 (2012).
 - [23] C. J. Feng, X. Y. Shen, P. Li and X. Z. Li, *A New Class of Parametrization for Dark Energy without Divergence*, JCAP **1209**, 023 (2012).
 - [24] E. Di Valentino, A. Melchiorri and J. Silk, *Reconciling Planck with the local value of H_0 in extended parameter space*, Phys. Lett. B **761**, 242 (2016).
 - [25] G. B. Zhao et al., *Dynamical dark energy in light of the latest observations*, Nat. Astron. **1**, 627 (2017).
 - [26] E. Di Valentino, A. Melchiorri, E. V. Linder and J. Silk,

- Constraining Dark Energy Dynamics in Extended Parameter Space*, Phys. Rev. D **96**, 023523 (2017).
- [27] E. Di Valentino, *Crack in the cosmological paradigm*, Nat. Astron. **1**, 569 (2017).
- [28] W. Yang, R. C. Nunes, S. Pan and D. F. Mota, *Effects of neutrino mass hierarchies on dynamical dark energy models*, Phys. Rev. D **95**, 103522 (2017).
- [29] M. Rezaei, M. Malekjani, S. Basilakos, A. Mehrabi and D. F. Mota, *Constraints to Dark Energy Using PADE Parameterizations*, Astrophys. J. **843**, no. 1, 65 (2017).
- [30] R. J. F. Marcondes and S. Pan, *Cosmic chronometers constraints on some fast-varying dark energy equations of state* [arXiv:1711.06157 [astro-ph.CO]].
- [31] W. Yang, S. Pan and A. Paliathanasis, *Latest astronomical constraints on some nonlinear parametric dark energy models*, Mon. Not. Roy. Astron. Soc. **475**, 2605 (2018).
- [32] M. Jaber and A. de la Macorra, *Probing a Steep EoS for Dark Energy with latest observations*, Astropart. Phys. **97**, 130 (2018).
- [33] S. Pan, E. N. Saridakis and W. Yang, *Observational Constraints on Oscillating Dark-Energy Parametrizations*, Phys. Rev. D **98**, no. 6, 063510 (2018).
- [34] S. Vagnozzi, S. Dhawan, M. Gerbino, K. Freese, A. Goobar and O. Mena, *Constraints on the sum of the neutrino masses in dynamical dark energy models with $w(z) \geq -1$ are tighter than those obtained in Λ CDM*, Phys. Rev. D **98**, no. 8, 083501 (2018).
- [35] X. D. Li *et al.*, *Cosmological Constraints from the Redshift Dependence of the AlcockPaczynski Effect: Dynamical Dark Energy*, Astrophys. J. **856**, no. 2, 88 (2018).
- [36] G. Panotopoulos and Á. Rincón, *Growth index and statefinder diagnostic of Oscillating Dark Energy*, Phys. Rev. D **97**, no. 10, 103509 (2018).
- [37] L. G. Jaime, M. Jaber and C. Escamilla-Rivera, *New parametrized equation of state for dark energy surveys*, Phys. Rev. D **98**, no. 8, 083530 (2018).
- [38] W. Yang, S. Pan, E. Di Valentino, E. N. Saridakis and S. Chakraborty, *Observational constraints on one-parameter dynamical dark-energy parametrizations and the H_0 tension*, arXiv:1810.05141 [astro-ph.CO].
- [39] W. Yang, S. Pan, E. Di Valentino and E. N. Saridakis, *Observational constraints on dynamical dark energy with pivoting redshift*, arXiv:1811.06932 [astro-ph.CO].
- [40] F. Pace, C. Schimd, D. F. Mota and A. Del Popolo, *Halo collapse: virialization by shear and rotation in dynamical dark-energy models*, arXiv:1811.12105 [astro-ph.CO].
- [41] M. Du, W. Yang, L. Xu, S. Pan and D. F. Mota, *Future Constraints on Dynamical Dark-Energy using Gravitational-Wave Standard Sirens*, arXiv:1812.01440 [astro-ph.CO].
- [42] D. Tamayo and J. A. Vazquez, *Fourier series expansion of the dark energy equation of state*, arXiv:1901.08679 [astro-ph.CO].
- [43] V. F. Mukhanov, H. A. Feldman and R. H. Brandenberger, *Theory of cosmological perturbations*, Phys. Rept. **215**, 203 (1992).
- [44] C. P. Ma and E. Bertschinger, *Cosmological perturbation theory in the synchronous and conformal Newtonian gauges*, Astrophys. J. **455**, 7 (1995).
- [45] K. A. Malik and D. Wands, *Cosmological perturbations*, Phys. Rept. **475**, 1 (2009).
- [46] N. Dimakis, A. Karagiorgos, A. Zampeli, A. Paliathanasis, T. Christodoulakis and P. A. Terzis, *General Analytic Solutions of Scalar Field Cosmology with Arbitrary Potential*, Phys. Rev. D **93**, 123518 (2016).
- [47] R. Adam *et al.* [Planck Collaboration], *Planck 2015 results. I. Overview of products and scientific results*, Astron. Astrophys. **594**, A1 (2016).
- [48] N. Aghanim *et al.* [Planck Collaboration], *Planck 2015 results. XI. CMB power spectra, likelihoods, and robustness of parameters*, Astron. Astrophys. **594**, A11 (2016).
- [49] M. Betoule *et al.* [SDSS Collaboration], *Improved cosmological constraints from a joint analysis of the SDSS-II and SNLS supernova samples*, Astron. Astrophys. **568**, A22 (2014).
- [50] F. Beutler *et al.*, *The 6dF Galaxy Survey: Baryon Acoustic Oscillations and the Local Hubble Constant*, Mon. Not. Roy. Astron. Soc. **416**, 3017 (2011).
- [51] A. J. Ross, L. Samushia, C. Howlett, W. J. Percival, A. Burden and M. Manera, *The clustering of the SDSS DR7 main Galaxy sample $\hat{a}\in I$. A 4 per cent distance measure at $z = 0.15$* , Mon. Not. Roy. Astron. Soc. **449**, no. 1, 835 (2015).
- [52] H. Gil-Marín *et al.*, *The clustering of galaxies in the SDSS-III Baryon Oscillation Spectroscopic Survey: BAO measurement from the LOS-dependent power spectrum of DR12 BOSS galaxies*, Mon. Not. Roy. Astron. Soc. **460**, no. 4, 4210 (2016).
- [53] D. M. Scolnic *et al.*, *The Complete Light-curve Sample of Spectroscopically Confirmed SNe Ia from Pan-STARRS1 and Cosmological Constraints from the Combined Pantheon Sample*, Astrophys. J. **859**, no. 2, 101 (2018).
- [54] M. Moresco *et al.*, *A 6% measurement of the Hubble parameter at $z \sim 0.45$: direct evidence of the epoch of cosmic re-acceleration*, JCAP **1605**, no. 05, 014 (2016).
- [55] A. Lewis and S. Bridle, *Cosmological parameters from CMB and other data: A Monte Carlo approach*, Phys. Rev. D **66**, 103511 (2002).
- [56] A. Lewis, A. Challinor and A. Lasenby, *Efficient computation of CMB anisotropies in closed FRW models*, Astrophys. J. **538**, 473 (2000).
- [57] A. Gelman and D. Rubin, *Inference from iterative simulation using multiple sequences*, Statistical Science **7**, 457 (1992).
- [58] N. Aghanim *et al.* [Planck Collaboration], *Planck 2018 results. VI. Cosmological parameters*, arXiv:1807.06209 [astro-ph.CO].
- [59] P. A. R. Ade *et al.* [Planck Collaboration], *Planck 2015 results. XIII. Cosmological parameters*, Astron. Astrophys. **594**, A13 (2016) [arXiv:1502.01589 [astro-ph.CO]].
- [60] A. G. Riess *et al.*, *A 2.4% Determination of the Local Value of the Hubble Constant*, Astrophys. J. **826**, no. 1, 56 (2016) [arXiv:1604.01424 [astro-ph.CO]].
- [61] A. Heavens, Y. Fantaye, A. Mootoovaloo, H. Eggers, Z. Hosenie, S. Kroon and E. Sellentin, *Marginal Likelihoods from Monte Carlo Markov Chains*, arXiv:1704.03472 [stat.CO].
- [62] A. Heavens, Y. Fantaye, E. Sellentin, H. Eggers, Z. Hosenie, S. Kroon and A. Mootoovaloo, *No evidence for extensions to the standard cosmological model*, Phys. Rev. Lett. **119**, no. 10, 101301 (2017).
- [63] R. E. Kass and A. E. Raftery, *Bayes Factors*, J. Am. Statist. Assoc. **90**, no.430, 773 (1995).
- [64] J. Aguirre *et al.* [Simons Observatory Collaboration], *The Simons Observatory: Science goals and forecasts*, JCAP **1902**, 056 (2019).
- [65] M. H. Abitbol *et al.* [CMB-S4 Collaboration], *CMB-S4*

- Technology Book, First Edition*, arXiv:1706.02464 [astro-ph.IM].
- [66] R. Laureijs *et al.* [EUCLID Collaboration], *Euclid Definition Study Report*, arXiv:1110.3193 [astro-ph.CO].
- [67] R. Scaramella *et al.* [Euclid Collaboration], *Euclid space mission: a cosmological challenge for the next 15 years*, IAU Symp. **10**, 375 (2014).
- [68] A. Aghamousa *et al.* [DESI Collaboration], *The DESI Experiment Part I: Science, Targeting, and Survey Design*, arXiv:1611.00036 [astro-ph.IM].
- [69] J. A. Newman *et al.* [LSST Dark Energy Science Collaboration], *Deep Multi-object Spectroscopy to Enhance Dark Energy Science from LSST*, arXiv:1903.09325 [astro-ph.CO].
- [70] R. A. Hložek *et al.* [LSST Dark Energy Science Collaboration], *Single-object Imaging and Spectroscopy to Enhance Dark Energy Science from LSST*, arXiv:1903.09324 [astro-ph.CO].
- [71] R. Mandelbaum *et al.* [LSST Dark Energy Science Collaboration], *Wide-field Multi-object Spectroscopy to Enhance Dark Energy Science from LSST*, arXiv:1903.09323 [astro-ph.CO].
- [72] H. Audley *et al.* [LISA Collaboration], *Laser Interferometer Space Antenna*, arXiv:1702.00786 [astro-ph.IM].
- [73] S. Kawamura *et al.*, *The Japanese space gravitational wave antenna: DECIGO*, Class. Quant. Grav. **28**, 094011 (2011).
- [74] S. Sato *et al.*, *The status of DECIGO*, J. Phys. Conf. Ser. **840**, no. 1, 012010 (2017).
- [75] J. Luo *et al.* [TianQin Collaboration], *TianQin: a spaceborne gravitational wave detector*, Class. Quant. Grav. **33**, no. 3, 035010 (2016).